Thermal Stability of Filtered Vacuum Arc Deposited Er$_2$O$_3$ Coatings

I. Zukerman[1,3,*], E. Goldenberg[1,2], V.N. Zhitomirsky[1,#], A. Raveh[4] and R.L. Boxman[1]

[1]*Electrical Discharge and Plasma Laboratory, Department of Physical Electronics, Tel-Aviv University, Tel-Aviv 69978, Israel*

[2]*UNAM – National Nanotechnology Research Center, Bilkent University, Ankara 06800, Turkey*

[3]*NRC-Negev, P.O. Box 9001, Beer-Sheva 84190, Israel*

[4]*Advanced Coatings Center, Rotem Industries Ltd., Mishor Yamin, D.N., Arava 86800, Israel*

Abstract: Erbium oxide (Er$_2$O$_3$) coatings were deposited using filtered vacuum arc deposition (FVAD) and their structure and thermal stability were studied as a function of fabrication parameters. The coatings were deposited on silicon wafer and tantalum substrates with an arc current of 50 A and a deposition rate of 1.6 ± 0.4 nm/s. The arc was sustained on truncated cone Er cathodes. The influence of oxygen pressure (P= 0.40-0.93 Pa), bias voltage (V_b= -20, -40 or grounded) and substrate temperature (room temperature (RT) or 673K) on film properties was studied before and after post deposition annealing (1273K for 1 hour, at $P\sim$ 1.33 Pa). The coatings were characterized using X-ray diffraction (XRD), optical microscopy, scanning electron microscopy (SEM), X-ray photoelectron spectroscopy (XPS) and Knoop Hardness.

Optical microscope images indicated that the coatings had very low macroparticle concentration on their surface. The macroparticle diameters were less than 2.5 µm. The coatings were composed of only Er$_2$O$_3$ without any metallic phase under all deposition parameters tested. The coatings deposited on RT substrates were XRD amorphous and had a featureless cross-section microstructure. However, the coatings deposited on 673K heated substrates had a C-Er$_2$O$_3$ structure with (222) preferred orientation and weak columnar microstructure. The coating hardness varied with deposition pressure and substrate bias, and reached a maximum value of 10 GPa at P = 0.4 Pa and V_b = -40 V. The post-deposition annealing caused crystallization, and the coatings hardness dropped to 4 GPa with thermal treatment. However, after post-deposition annealing, no peeling or cracking appeared at the coating surface or the interface with the substrate.

[#]***This paper is dedicated to our colleague Dr. Vladimir Zhitomirsky who initiated this investigation and passed away during the study.***

1. INTRODUCTION

Erbium oxide (Er$_2$O$_3$) is a rare-earth oxide with many attractive properties. It has high thermodynamic stability, high thermal stability, high dielectric constant, wide band gap, high photo response and low permeation of hydrogen isotopes. Thus, Er$_2$O$_3$ coating is a promising candidate for applications such as protective coatings at fusion power plants [1, 2], high dielectric gate material as a replacement for SiO$_2$ gate insulators [3] and optoelectronic applications [4].

Er$_2$O$_3$ can be deposited using various methods, including laser ablation [4], electron-beam evaporation [3], sol-gel and metal-organic decomposition [5], metal-organic chemical vapor deposition [2], magnetron sputtering [6] and filtered vacuum arc deposition, FVAD [1,7]. Among these techniques, FVAD is promising, because its plasma produces coatings with higher packing density and better adhesion than other techniques, due to high-energy metal plasma ions impinging the coated substrate.

Er$_2$O$_3$ coatings usually have a C-phase, cubic structure [3, 6, 7], which is the stable phase below 2600K and at ambient pressure. Monoclinic, B-phase Er$_2$O$_3$ was reported by both Adelhelm *et al.* [7] and Li *et al.* [5] who used FVAD and pulsed magnetron sputtering, respectively. In both cases, B-Er$_2$O$_3$ was formed when the coatings were deposited at low deposition temperatures (<673K), under ion bombardment and at high deposition rates (~0.8 nm/s). These conditions reduced surface diffusion and induced high residual stress [6, 7]. After annealing, the B–phase coatings transformed to C-Er$_2$O$_3$ [6, 7]. The mechanical properties of the Er$_2$O$_3$ coatings were almost never studied, although they are important for

[*]NRC-Negev, P.O. Box 9001, Beer-Sheva 84190, Israel; Tel: 972-8-6567205; Fax: 972-8-6568686; E-mail: idozukerman@gmail.com

the coating to be able to withstand handling and wear. FVAD *C*-phase Er_2O_3 coatings had hardness of *H*= 24 GPa and reduced Young's modulus of *E**= 308 GPa, while *C*-Er_2O_3 deposited using pulsed magnetron sputtering had lower values of *H*= 16.2 and *E**= 216 GPa. *B*-Er_2O_3 coatings had lower *H* and *E** values [6].

Previously, Zhitomirsky *et al.* [8] reported on Er_2O_3 coatings deposited using a non-filtered vacuum arc with a relatively (for Er_2O_3) high hardness of 14 ± 1 GPa. However, the presence of macro-particles complicated the coating characterization. The deuterium permeation and dielectric constant of Er_2O_3 have been studied by many investigators. However, structure and thermal stability as well as their dependence on fabrication parameters need further study. In this study, we report on the FVAD Er_2O_3 coating hardness, microstructure and composition before and after thermal annealing at 1273K. Additionally, we studied the effect of the oxygen pressure, substrate bias and temperature on the coatings properties.

2. EXPERIMENTAL SET-UP AND PROCEDURE

A schematic diagram of the filtered vacuum arc deposition (FVAD) system is shown in Figure **1**. The FVAD system is comprised of the following main components: a plasma gun, a quarter-torus magnetic macroparticle filter, a deposition chamber with a gate valve and load-lock chamber, a vacuum system with diffusion and rotation pumps and a control system based on PC data acquisition controllers and a Labview program [9]. The arc plasma source consisted of a water-cooled Er cathode, an annular water-cooled 30 mm aperture Cu anode, a spacer, and a trigger. The cathode had a frustum cone shape with base diameters of 16.5 and 25 mm, and a height of 13 mm as described elsewhere [8]. The plasma source was mounted on a quarter torus magnetic MP

filter with a 240 mm major radius and a 80 mm minor radius (toroidal duct diameter 160 mm). The toroidal magnetic field (*BT*) was generally parallel to the torus wall. Usually, the dc current applied to the toroidal coils (to guide the plasma through the duct) was 2-3 A and *BT*= 12-18 mT. More details about this system can be found in previous publications [9].

The samples were prepared on silicon (Si) and tantalum (Ta) substrates (10×20 mm). The coatings which were deposited on Si substrates were used to study the fracture cross-section, while the coatings deposited on the Ta substrates were used for structural, chemical and mechanical study of the Er_2O_3 layers. Before arc ignition, the vacuum chamber was pumped down to an initial residual pressure lower than 0.01 Pa. Arc current, I_{arc}= 50 A d.c. was applied between the cathode and the grounded anode. The arcs were operated in oxygen background pressure of *P*= 0.40–0.93 Pa and a negative d.c. bias voltage of V_b= 0 − 40 V was applied to the substrate holder. Most of the coatings were deposited on room temperature (RT) substrates, but some were performed at *T*= 673K. The duration of each deposition process was *t*= 360 s. After deposition, some of the coated samples were annealed in vacuum (~1.33 Pa) at a temperature of 1273K for an hour.

The coating surface and cross section morphology, and the film thickness, were determined using a scanning electron microscope (SEM JSM-6300). The elemental distribution and oxidation status of elements in the coatings were evaluated by using a 5600 AES/XPS Multi-Technique System (PHI, USA). X-ray diffraction (XRD) patterns were recorded using a symmetric Bragg geometry 'Scintag' powder diffractometer equipped with a Cu Kα (wavelength λ= 0.1541 nm) radiation source, and a liquid-nitrogen-cooled Ge solid-state detector. The texture, *T** was calculated from the following equation in accordance with the Harris inverse pole technique [10]:
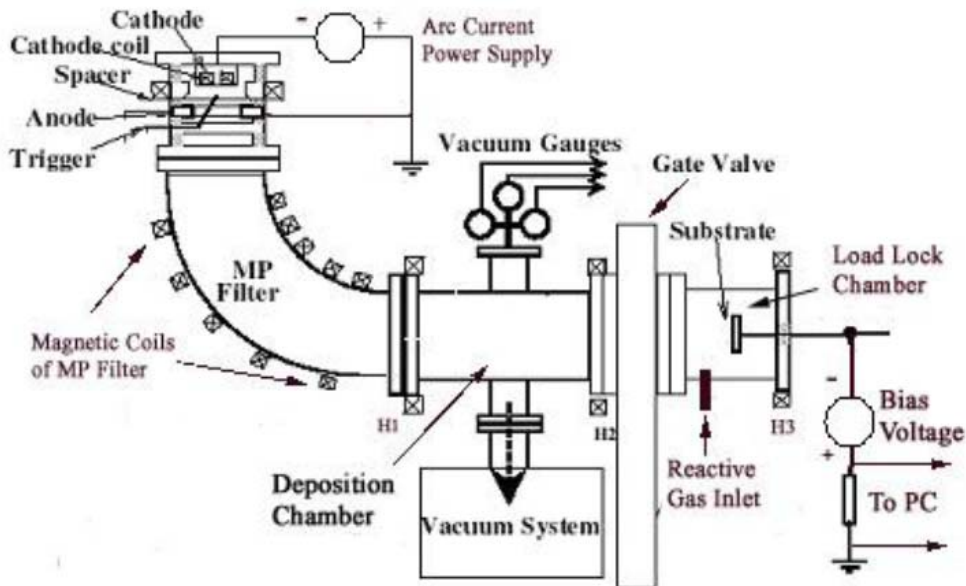

Figure 1: Schematic diagram of the FVAD system.

$$T* = \frac{I_{hkl} / R_{hkl}}{(1/n)\sum_{o}^{n} I_{hkl} / R_{hkl}}$$

(1)

Where, I_{hkl} and R_{hkl} are the intensities from the (*hkl*) reflections in the sample and random powder, respectively, and *n* is the number of reflections. The grain size, *D*, was calculated from Scherrer's equation [11]. The coating hardness, H_K, was measured using a microhardness tester equipped with a Knoop indenter at various loads and then calculated using the model described by Lost [12].

3. RESULTS

3.1. Properties of as-Deposited Coatings

All coatings deposited in this work were visually transparent and smooth, without any cracks or spelling. However, coatings deposited at $P \leq 0.4$ Pa and with $V_b \geq$ -20 V, had arc tracks on the coating surface, which caused to a rough surface morphology. When the pressure increased to $P \leq$ 0.53, the arc tracks appeared only when $V_b \geq$ -40 V. The coatings thickness, measured using SEM fracture cross-sections, was in the range of 0.5-0.9 μm without any

correlation to the deposition conditions (*P*, V_b or substrate temperature). The variation of the coating thickness can be explained by collimated FVAD plasma beam, and the difficulty in measuring the coating thickness at the same position relative the plasma beam. The deposition rate was estimated to be 1.6 ± 0.4 nm/s.

Figure **2a,c** presents typical SEM images of coatings deposited on RT substrates. For comparison, Figure **2b** presents an optical microscope image of Er_2O_3 coating deposited in our lab using non-filtered VAD system [8]. The Er_2O_3 coating surface deposited during the current work (using FVAD) was smooth and without cracks or voids (Figure **2a**). At the coating surface, one can see a low concentration of small metallic Erbium droplets (i.e. with a rich Erbium concentration as identified by SEM-EDX). These macro-particles were smaller than 2.5 μm and were considerably smaller and fewer than in the coatings deposited using non-filtered VAD (Figure **2b**) [8]. The coating cross-section (Figure **2c**) was featureless, and specifically did not have a columnar structure. The coatings had a continuous interface with the substrate, without any cracks or voids. This usually signifies good adhesion. All coatings
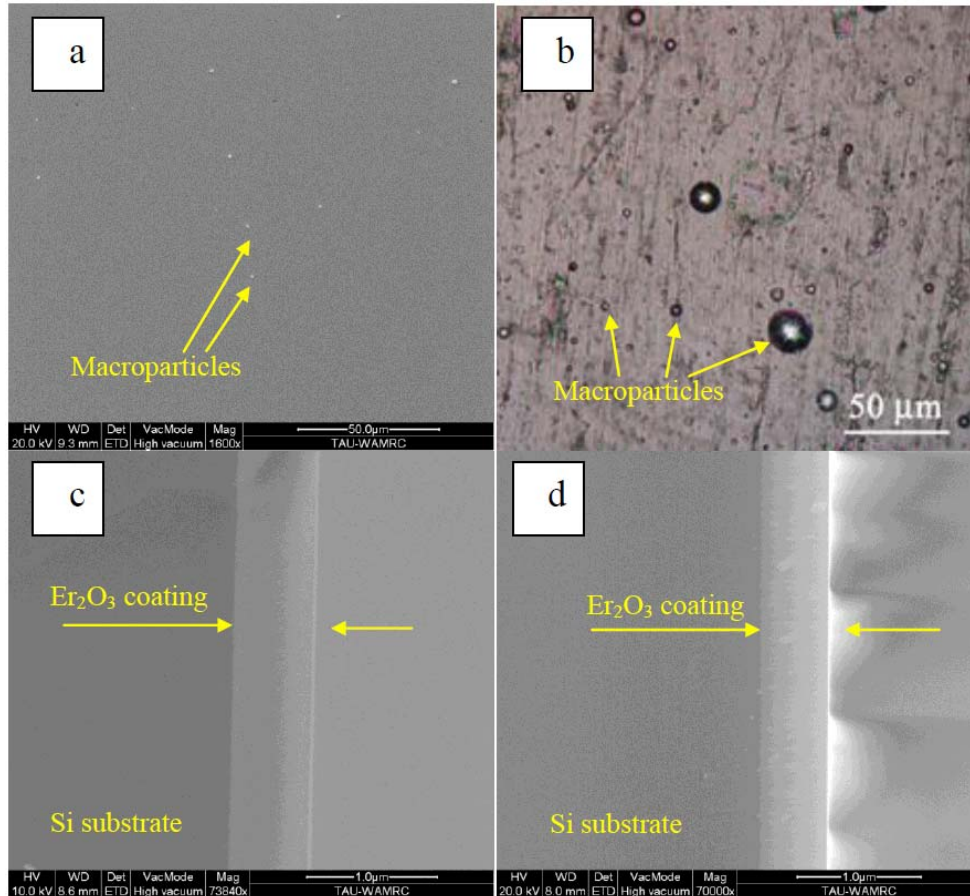

Figure 2: SEM images of Er_2O_3 coatings deposited using FVAD: **a**) typical surface image of Er_2O_3 coatings deposited on RT substrates, **b**) optical microscope image typical to coatings deposited in previuos work using a non-filtered VAD system [23], **c**) typical cross section view of Er_2O_3 coatings deposited on RT substrates **d**) cross section view of Er_2O_3 coating deposited on 673K substrates. FVAD parameters (for **a**, **b** and **d**): I_{arc}= 50 A, *P*= 0.66 Pa, V_b= -20 V (on RT substrates) and grounded (on 673K substrates), *t* = 360 s. VAD parameters (for c): I_{arc} = 50 A, *P* = 0.66 Pa, V_b = -40 V, *t* = 60 s.
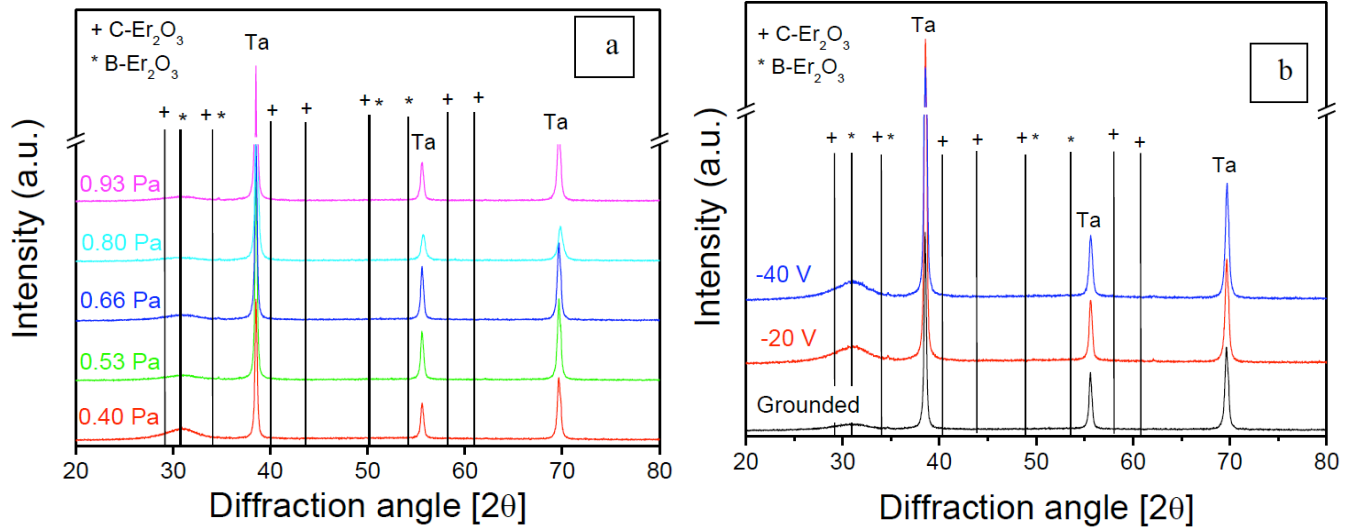
Figure 3: XRD patterns of as-deposited Er_2O_3 coatings as a function of (**a**) P at V_b = grounded and (**b**) V_b at P = 0.67 Pa.

deposited at room temperature (independent to P or V_b), had similar features to the ones presented in Figures **2a,c**. Deposition on 673K substrates had the same coating surface morphology (similar to Figure **2a**) but in the cross-section pictures, a weak columnar structure was observed (Figure **2d**).

Figures **3a-b** presents XRD diffraction patterns from Er_2O_3 coatings deposited on RT substrates, at various P and V_b, respectively. The solid vertical lines represent the theoretical positions of the major C- and B-Er_2O_3 XRD peaks. All coatings deposited on RT substrates and, regardless of P or V_b, were almost XRD amorphous with a very broad peak at 30°. This peak can be associated to a number of B-Er_2O_3 peaks [6]. The intensity of the 30° peak increased with V_b and decreased with P. When the coatings were deposited on 673K heated substrates, a strong crystallographic structure was identified (Figure **4**). The coatings had mainly C-Er_2O_3 structure with strong {111} preferred orientation (Table **1**) and a minor B-phase, as indicated from the presence of 26.4° and 30° peaks. The coatings grain size was calculated using Scherrer's equation and was found to be 200 ± 50 nm.
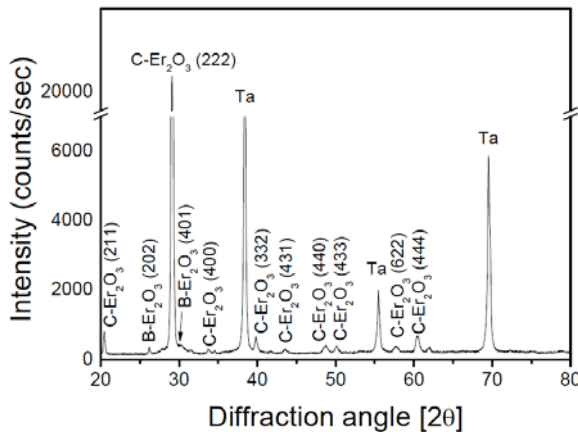

Figure 4: XRD diffraction patterns of Er_2O_3 coatings deposited on 673K substrates at P = 0.67 Pa and V_b= grounded.

Figure **5** presents high-resolution XPS spectra of Er 3d in coatings deposited on RT substrates with different P and V_b. The spectra were taken after surface contamination was etched away using 10 min of Ar^+ ion sputtering. The Er 3d peak (Figure **5**) is similar in shape to pure Er_2O_3 [13], although the peak position is at a lower binding energy than obtained by Tewell and King [12]. Table **2** presents the Er:O atomic concentration ratio calculated using the XPS data. All coatings showed over-stoichiometric oxygen, which increased with P. This apparent over-stoichiometric oxygen could be attributed to an inaccurate atomic sensitivity factor [14].

Figure **6** presents the coatings hardness as function of P, V_b and substrate temperature. When the coatings were deposited with V_b= -20 V, H_K was ~7 GPa, regardless to P. On the other hand, when V_b= -40 V, the hardness decreased from H_k= 10 GPa at P= 0.53 Pa to HK= 4.9 GPa at P= 0.93 Pa. Deposition on 673K heated substrates resulted in low hardness, H_k= 4.1 GPa.

3.2. The Effect of Post-Deposition Annealing

The Er_2O_3 coatings were annealed in vacuum (~1.33 Pa) at 1273K for 1 hour. The annealing changed the crystallographic structure of all coating deposited on RT substrates form nearly amorphous (Figure **3**) to crystalline C-Er_2O_3 (Figure **7**). The latter diffraction data is typical of all annealed coatings on RT substrates. No B-Er_2O_3 peaks were found in the post-annealing XRD patterns. Texture analysis (Table **1**) showed that the annealed coatings did not have preferred orientation, although the coatings had dominant {211}, {111} and {332} crystallographic planes. For coatings deposited on 673K heated substrates, the annealing increased the peak intensity, while keeping and increasing their {111} preferred orientation (Table **1**). The coatings grain size, after annealing, was 450 ± 50 nm and 380 ± 50 nm for coatings deposited at RT and T= 673 K, respectively.

Table 1:   Texture Parameter of Er$_2$O$_3$ Coatings

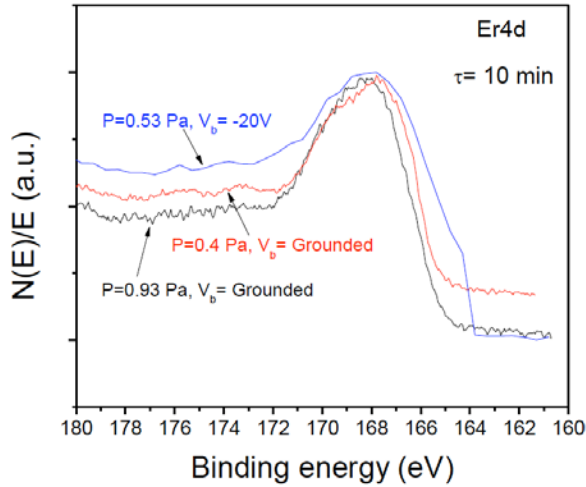| Coating Parameter				Texture Parameter T^*								
P [Pa]	T [K]	V_b [V]		{211}	{111}	{100}	{411}	{332}	{413}	{110}	{311}	{613}
0.67	673	0	As- deposited	1.14	4.75	0.05	0.00	2.16	0.21	0.09	0.08	0.00
0.67	673	0	Annealed	0.95	5.29	0.03	0.00	2.12	0.17	0.08	0.08	0.00
0.93	RT	-20		1.83	1.96	0.85	1.21	1.73	1.04	0.84	0.47	0.61
0.66	RT	-20		2.49	2.43	1.29	1.29	2.29	1.40	1.10	0.60	0.89
0.66	RT	-40		1.96	2.06	1.01	1.33	2.16	1.22	1.00	0.47	0.65
0.93	RT	-40		1.97	2.31	0.77	1.18	1.49	1.08	0.99	0.52	0.64

Figure 5: High resolution XPS scans of the Er 3d line in Er$_2$O$_3$ coatings deposited on RT substrates.

Table 2:   Elemental Composition of Er$_2$O$_3$ Coatings Obtained from XPS Measurements as a Function of Oxygen Pressure. All Coatings were Deposited at RT. Measurement Accuracy was 2-5%

O$_2$ pressure [Pa]	0.4	0.53	0.93
Substrate bias [V]	Grounded	-20	Grounded
O [at.%]	70.59	76.06	80.08
Er [at.%]	29.41	23.94	19.92
Er:O ratio	1:2.38	1:3.22	1:4.0

Study of the interface between the Er$_2$O$_3$ coatings and the Ta or Si substrates showed a sharp interface and good adhesion. Although annealing changed the RT coatings structure from amorphous to crystalline (Figure **7**), their cross-section SEM images remained featureless (similar to Figure **2c**), regardless to P or V_b. The coatings deposited on 673K heated substrates had a strong columnar microstructure after annealing (Figure **8**). The hardness of all annealed coatings was low i.e. H_k= 4 ± 0.5 GPa, regardless of the deposition parameters or their hardness before annealing.

4. DISCUSSION

Erbium oxide coatings were deposited using FVAD at various P and Vb. The deposition rate in the present work was 1.6 ±

0.4 nm/s using a 50 A arc. This rate is an order of magnitude lower than obtained with the same cathode gun but without macroparticle filtering [8], which is a typical decrease when a quarter-torus filter is used [15]. The deposition rate presented in this paper is higher than reported by Adelhelm *et al*. [7], however it is similar to the deposition rates reported, previously, using the present FVAD system [9]. The high deposition rate can be explained by focused nature of the Er
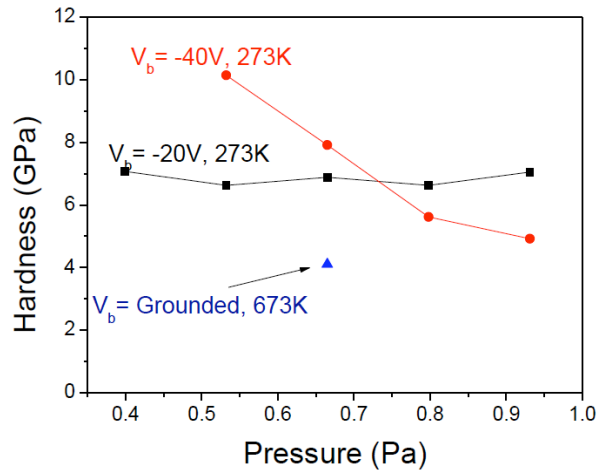

Figure 6: Coating hardness as a function of P, V_b and substrate temperature.
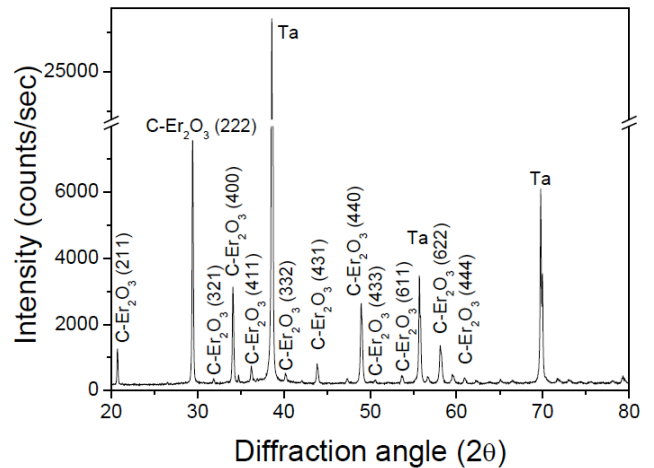

Figure 7: XRD diffraction patterns of Er$_2$O$_3$ coatings deposited at RT and annealed for 1 hour at 1273K. Deposition parameters: P = 0.67 Pa and V_b = -20 V.

plasma beam [8]. While the high deposition rate was convenient for allowing a relatively short sample turn-around time, the high plasma density together with application of a bias voltage, produced a high field at the substrate surface which could produce electrical breakdown and arcing on the sample [16]. To prevent arcing, deposition conditions were limited to relatively low V_b at the following regimes: V_b= -20 V, P≤ 0.4 Pa or V_b= -40 V, P≤ 0.53 Pa.
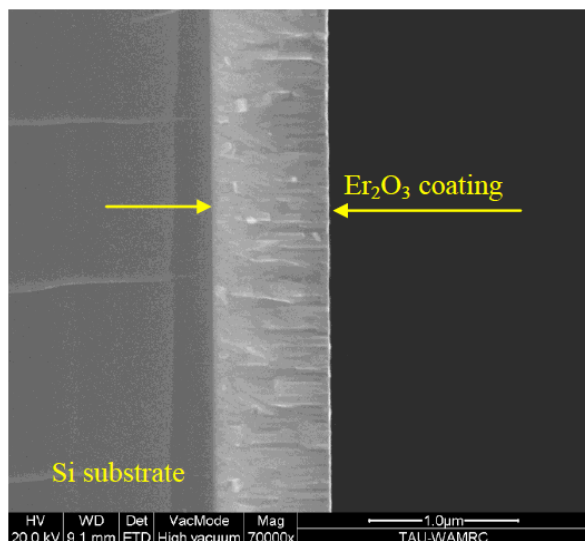

Figure 8: SEM cross-section images of Er_2O_3 coatings deposited at P = 0.66 Pa, V_b= grounded and 673K substrates, later annealed at 1273K for an hour. The dark layer under the coating-substrate interface is an artifact from the fracture.

The high deposition rate together with low deposition temperature hinder crystallization [17], resulting in an almost amorphous XRD patterns with very broad peak at 30º (Figure **3**). In the case of deposition on RT substrates, the energy needed for crystallization is delivered by the ions impinging the surface. Thus, as V_b increased (Figure **3b**), the intensity of the 30° peak increased, while as P increased the same peak decreased (Figure **3a**), due to higher probability for collisions with the gas atoms. Adelhelm *et al.* [7] deposited *B*-Er_2O_3 coatings on RT substrates, but with lower deposition rate and much higher V_b (> -100 V), while their coatings deposited on RT substrates with V_b = 0 V had lower crystallinity.

The formation of *B*-Er_2O_3 on RT substrates is explained by the high deposition rate and low ad-atom mobility, quenching the *B*-phase. Another explanation is the formation of high compressive stress due to ion bombardment [7]. Crystallization of *C*-Er_2O_3 coatings using non-plasma methods e.g. CVD, usually occurs at ~773K [2]. Jankowski *et al.* [3] deposited using e-beam evaporation and reported a mixture of *B*- and *C*-phases when the substrate temperature was >665K, transforming to only *C*-phase at ≥948K. Li *et al.* [6] used mid-frequency (40 kHz) pulsed magnetron sputtering and reported a transformation from *B*-phase to *C*-phase at a deposition temperature of 773K, although they did not state the substrate potential (grounded, floating or biased). In our

study, we deposited *C*-Er_2O_3 coatings (with very low content of *B*-Er_2O_3) on 673K heated substrates (V_b grounded). This temperature is lower than the one reported by Adelhelm *et al.* [7] for full transformation (873K). The high ion fluxes in our work (as can be assumed from the high deposition rate) deliver energy to the surface and can reduce the crystallization temperature.

Although V_b had little affected the coating crystalline structure, it did affect the coating hardness. The bulk hardness of Er_2O_3 is about 7 GPa [18], which is about the hardness of coatings deposited with V_b= -20V. However, when V_b was -40 V, H_K varied with P, with the highest hardness, H_K= 10 GPa at the lowest pressure, P= 0.40 Pa and the lowest hardness of H_K= 4 GPa at the highest pressure, P= 0.93 Pa. The increase in hardness with V_b is well known and is usually comes with an increase in compressive intrinsic stress [6, 19]. The decrease in hardness with P is less understood. We believe that at a regime of high P and V_b there is implantation of oxygen in the Er_2O_3 coating (producing an over-stoichometric composition, see Table **2**) which reduces the hardness. Another possible explanation could be a decrease in the energy of the impinging ions, due to collisions with gas molecules, although, in that case, we would expect similar decrease with P at V_b= -20 V. The decrease in post-annealing coatings hardness to H_K~ 4 GPa, regardless of their as-deposited hardness, suggests that the as-deposited hardness was originated from, 1) nanocrystalline structure or 2) residual stress [18]. In both cases the annealing induced grain growth, stress release by different recovery mechanisms [19] or both which in turn resulted in sharp decrease in hardness. The reason for the relatively low hardness of the coatings in this work is not clearly understood and needs further work. However, the annealing process did not cause to any delamination, which indicates good adhesion.

5. CONCLUSIONS

Er_2O_3 coatings deposited using FVAD on RT substrates had a nearly-amorphous structure, with only a weak *B*-Er_2O_3 signature. In contrast, coatings deposited on 673K heated substrates had a *C*-Er_2O_3 structure with (222) preferential orientation. The coating crystallinity was increased with the substrate bias and decreased with the oxygen pressure during deposition. The coating hardness was determined by a combination of oxygen pressure and substrate bias. The maximum hardness of ~10 GPa was achieved with the highest bias (V_b= -40 V) and lowest pressure (0.4 Pa) tested in this work. Thermal annealing crystallized the coatings to *C*-Er_2O_3 but also softened the coating. The Er_2O_3 coatings sustained a thermal cycle of 1273K without cracking or delaminating.

REFERENCES

[1]   Levchuk D, Levchuk S, Maier H, Bolt H, Suzuki A. Erbium oxide as a new promising tritium permeation barrier. J Nucl Mater 2007; 367-370: 1033-7.
http://dx.doi.org/10.1016/j.jnucmat.2007.03.183

[2] Hishinuma Y, Tanaka T, Tanaka T, *et al.* Investigation of Er$_2$O$_3$ coating on liquid blanket components synthesized by the MOCVD process. J Nucl Mater 2011; 417: 1214-7.
http://dx.doi.org/10.1016/j.jnucmat.2010.12.282

[3] Jankowski AF, Saw CK, Ferreria JL, Harper JS, Hayes JP, Pint BA. Morphology, microstructure, and residual stress in EBPVD erbia coatings. J Mater Sci 2007; 42: 5722-7.
http://dx.doi.org/10.1007/s10853-006-0658-7

[4] Grishin AM, Vanin EV, Tarasenko OV, Khartsev SI, Johansson P. Strong broad C-band room temperature photoluminescence in amorphous Er$_2$O$_3$ films. Appl Phys Lett 2006; 89: 021114.
http://dx.doi.org/10.1063/1.2221517

[5] Chikada T, Suzuki A, Tanaka T, Terai T, Muroga T. Microstructure control and deuterium permeability of erbium oxide coating on ferritic/martensitic steels by metal-organic decomposition. Fusion Eng Des 2010; 85: 1537-41.
http://dx.doi.org/10.1016/j.fusengdes.2010.04.033

[6] Li X, Wu P, Qiu H, Chen S, Songm B. Crystallization behavior and mechanical properties of erbium oxide coatings fabricated by pulsed magnetron sputtering. Thin Solid Films 2012; 520: 2316-20.
http://dx.doi.org/10.1016/j.tsf.2011.09.053

[7] Adelhelm C, Pickert T, Koch F, *et al.* Influence of deposition temperature and bias voltage on the crystalline phase of Er$_2$O$_3$ thin films deposited by filtered cathodic arc. J Nuc Mater 2011; 417: 798-801.
http://dx.doi.org/10.1016/j.jnucmat.2010.12.163

[8] Zhitomirsky VN, Raveh A, Boxman RL, Goldsmith S. Vacuum arc plasma beam produced from erbium cathode. IEEE Trans Plasma Sci 2009; 37: 1517-22.
http://dx.doi.org/10.1109/TPS.2009.2024671

[9] Çetinörgü-Goldenberg E, Burstein L, Chayun-Zucker I, Avni R, Boxman RL. Structural and optical characteristics of filtered vacuum arc deposited N:TiOx thin films. Thin Solid Films 2013; 537: 28-35.
http://dx.doi.org/10.1016/j.tsf.2013.04.116

[10] Harris GB, Quantitative measurement of preferred orientation in rolled uranium bars. Phil Mag 1952; 43: 113-23.
http://dx.doi.org/10.1080/14786440108520972

[11] Patterson A. The Scherrer Formula for X-Ray Particle Size Determination. Phys Rev 1939; 56; 978-82.
http://dx.doi.org/10.1103/PhysRev.56.978

[12] Lost A. Knoop hardness of thin coating. Scripta Materialia 1998; 39: 231-8.
http://dx.doi.org/10.1016/S1359-6462(98)00139-0

[13] Tewell CR, King SH. Observation of metastable erbium trihydride. App Surf Sci 2006; 253: 2597-602.
http://dx.doi.org/10.1016/j.apsusc.2006.05.025

[14] Zhang D, Tanaka T, Muroga T. Electrical resistivity and hydrogen permeation of dip-coated Er$_2$O$_3$ on JLF-1. J Nuc Mater 2011; 417: 1249-52.
http://dx.doi.org/10.1016/j.jnucmat.2010.12.281

[15] Boxman RL, Zhitomirsky VN. Vacuum arc deposition devices. Rev Sci Instrum 2006; 77: 021101.
http://dx.doi.org/10.1063/1.2169539

[16] Boxman RL. Triggering Mechanisms in Triggered Vacuum Gaps. IEEE Trans. Electron Devices 1977; ED-24: 122-8.
http://dx.doi.org/10.1109/T-ED.1977.18690

[17] Sanders DM, Anders A. Review of cathodic arc deposition technology at the start of the new millennium. Surf Coat Technol 2000; 133-4: 78-90.
http://dx.doi.org/10.1016/S0257-8972(00)00879-3

[18] Yeheskel O, Albayak IC, Anason B, Barsoum MW. Mechanical and elastic properties of fine-grained polycrystalline scandia and erbia as determined by indentation techniques. J Eur Cer Soc 2011; 31: 1708-12.
http://dx.doi.org/10.1016/j.jeurcermsoc.2011.03.030

[19] Karvankova P, Mannling HD, Eggs C, Veprek S. Thermal stability of ZrN–Ni and CrN–Ni superhard nanocomposite coatings. Surf Coat Technol 2001; 146-147: 280-5.
http://dx.doi.org/10.1016/S0257-8972(01)01477-3